Appendix D

ON-CHIP CLUSTER STATE GENERATION

To illustrate the potential of integrated optoelectronic systems for quantum information processing, we perform a proof-of-concept demonstration of cluster state generation in a measurement-based approach [1, 2] using the QPA system of Chapter 6. Cluster states are a class of entangled graph states that form a resource for universal measurement-based quantum computation [3]. Continuous-variable Gaussian cluster states can be generated by interfering squeezed states in linear optical networks [4, 5]. Here, we generate two-mode cluster state correlations by implementing a virtual linear optical network after optoelectronic downconversion with an RF circuit.

Cluster states of up to eight modes have been demonstrated with bulk multipixel homodyne detection systems by programming virtual optical networks in digital post-processing [1]. The virtual networks mix different spatial regions in a beam of light to match the detection basis to an entangled spatial mode basis. This method of entanglement generation allows for highly compact and versatile implementations of Gaussian quantum computation in the measurement-based model [2], which can be scaled to a higher number of modes by interfacing quantum PICs like the QPA chip with special-purpose RF or microwave ICs.

D.1 Experiment

The quantum circuit architecture used in the experiment is shown in Fig. D.1a. A squeezed state is transmitted over free space to the QPA chip, and a phase ramp at a modulation frequency of 0.5 Hz is applied to the LO before coupling it to the chip. The RF outputs of the QRXs in each half of the array are sent to a 16:1 power combiner. Beamforming is performed on all 32 channels such that the two outputs of the power combiners are in phase. To improve the geometric efficiency, the outermost 12 channels are disconnected from each 16:1 power combiner, for a total of 8 pixel modes in Fig. D.1a. The outputs of the power combiners are digitized at a sampling rate of 100 MSa/s, and an RF beamsplitter transformation is emulated on the digitized quadratures (see Methods).

With our architecture in Fig. D.1a, the overall transformation on the input field can

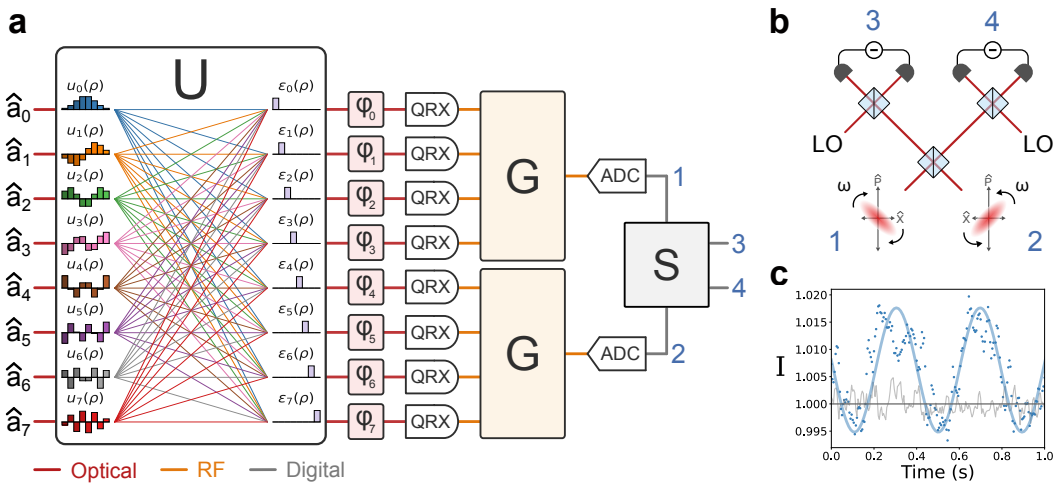

Figure D.1: Quantum optoelectronic processing. a) Optoelectronic circuit architecture for entanglement generation. The free space operation (U) corresponds to the change-of-basis matrix mapping the spatial modes of the input state to the pixel modes, where ρ represents the spatial coordinates in the aperture plane of the chip. Each colored line represents a matrix element corresponding to the overlap of an antenna and pixel mode function. A phase shifter φ_j is applied to each pixel mode, and each half of the array is combined in a 16:1 RF power combiner (G). The output voltages of the power combiners are digitized and followed by a beamsplitter transformation (S). b) Emulated optical circuit for two-mode Gaussian cluster state generation. c) The cluster state inseparability (I) measured over time for a linear phase ramp. The data for the squeezed vacuum and vacuum states are plotted in blue and gray, respectively. The solid lines are the analytical expectations with a sinusoidal fit to the squeezed data.

be summarized as,

$$\vec{a}_{\text{out}} = S(G \oplus G)DU\vec{a}_{\text{in}}, \tag{D.1}$$

where U is the free-space change-of-basis unitary mapping the input modes to pixel modes, $D = \text{diag}(e^{i\phi_1}, e^{i\phi_2}, ...)$,

$$G \oplus G = \begin{pmatrix} 1 & 1 & 1 & 1 & 0 & 0 & 0 & 0 \\ 0 & 0 & 0 & 0 & 1 & 1 & 1 & 1 \end{pmatrix} \tag{D.2}$$

is the gain matrix of the RF power combiners, and

$$S = \frac{1}{\sqrt{2}} \begin{pmatrix} 1 & i \\ i & 1 \end{pmatrix} \tag{D.3}$$

is the beamsplitter matrix. The transformation of S is performed on the digitized quadratures as an emulation of an RF directional coupler, where complex matrix elements are implemented as a $\pi/2$ phase shift. For a two-mode Gaussian cluster state generated with S, the cluster state correlations are given by,

$$\mathrm{Var}(\hat{Q}_3(\theta) - \hat{P}_4(\theta)) = \mathrm{Var}(\hat{Q}_1(\theta)), \tag{D.4}$$

$$\mathrm{Var}(\hat{Q}_4(\theta) - \hat{P}_3(\theta)) = \mathrm{Var}(\hat{Q}_2(\theta)), \tag{D.5}$$

where $\mathrm{Var}(\hat{Q}_i(\theta))$ for $i = 1, 2$ is given by,

$$\langle \Delta \hat{Q}_\theta^2 \rangle_{\mathrm{sq}} = \frac{\eta}{2}(e^{-2r}\cos^2\theta + e^{2r}\sin^2\theta) + \frac{1-\eta}{2},$$

for squeezed modes, such that the right-hand side is zero at $\theta = 0$ in the limit of large squeezing parameter and low loss. The inseparability criterion required to show cluster state entanglement is

$$I = \mathrm{Var}(\hat{P}_4 - \hat{Q}_3) + \mathrm{Var}(\hat{P}_3 - \hat{Q}_4) < 1, \tag{D.6}$$

where $\hat{Q}_i, \hat{P}_i$ are the quadrature operators for each cluster state mode denoted by $i = 3, 4$ in Fig. D.1b, and the variances are relative to those of the vacuum state.

The quadrature correlations I as a function of time are shown in Fig. D.1b. We observe the sinusoidal signature expected for a rotation of the measurement basis due to the LO phase modulation.

D.2 Cluster state inseparability

The minimum and maximum inseparability levels are estimated from the histograms of the inseparabilities with the procedure in Appendix B. The histogram and kernel density estimate of the data in D.1c is shown in Fig. D.2. The estimates for the min. and max. inseparabilities are 0.994 ± 0.002 and 1.018 ± 0.002, respectively. The sinusoidal fit in Fig. D.1c. is performed with the amplitude fixed by the minimum and maximum inseparability estimates and the angular frequency (ω) and phase (ϕ) taken as floating parameters. We obtain fit parameters of $\omega = 7.99 \pm 0.12$ and $\phi = 0.703 \pm 0.069$.

D.3 Discussion

We estimate a maximum inseparability of $I = 1.0176 \pm 0.0004$ and a minimum inseparability of $I = 0.9948 \pm 0.0004$. The resolution of the measured entanglement

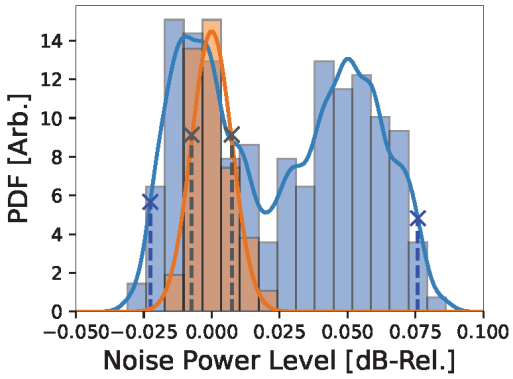

Figure D.2: Histogram of inseparability data in Fig. D.1c for squeezed vacuum (blue) and vacuum (orange) states. The solid blue and orange lines are the kernel density estimates. The min. and max. inseparability estimates are indicated with blue crosses. The vacuum standard deviations are indicated with black crosses.

is enabled by the high precision and stability offered by the chip-scale optoelectronics. We note that in our experiment, the inseparability given by Eq. D.6 has a lower bound of 0.5 since the squeezed light was generated in a single mode. This lower bound can be overcome by transmitting multiple squeezed modes to the chip, allowing for the generation of large cluster states up to 32 modes.

Our demonstration show the potential for optoelectronic systems on-chip for applications in quantum information processing. More broadly, integrating quantum photonics with electronics in the same package offers novel engineering opportunities in realizing large-scale room-temperature quantum systems. Coherent processing of downconverted quantum optical information with RF or microwave integrated circuits could enable compact and low-loss optoelectronic approaches to measurement-based quantum information processing, where certain linear operations are offloaded to electronics, as a generalization of classical microwave photonics [6].

References

[1] Seiji Armstrong, Jean-François Morizur, Jiri Janousek, Boris Hage, Nicolas Treps, Ping Koy Lam, and Hans-A Bachor. “Programmable multimode quantum networks.” In: Nature Communications 3.1 (2012), p. 1026.

[2] Giulia Ferrini, Jean-Pierre Gazeau, Thomas Coudreau, Claude Fabre, and Nicolas Treps. “Compact Gaussian quantum computation by multi-pixel homodyne detection.” In: New Journal of Physics 15.9 (2013), p. 093015.

[3] Robert Raussendorf and Hans J. Briegel. “A one-way quantum computer.” In: Physical Review Letters 86.22 (2001), p. 5188.

[4] Peter van Loock, Christian Weedbrook, and Mile Gu. “Building Gaussian cluster states by linear optics.” In: Physical Review A 76.3 (2007), p. 032321.

[5] Mitsuyoshi Yukawa, Ryuji Ukai, Peter Van Loock, and Akira Furusawa. “Experimental generation of four-mode continuous-variable cluster states.” In: Physical Review A 78.1 (2008), p. 012301.

[6] David Marpaung, Jianping Yao, and José Capmany. “Integrated microwave photonics.” In: Nature Photonics 13.2 (Feb. 2019), pp. 80–90.